WFPC2 Observations of NGC 454: an Interacting Pair of Galaxies [1]

M. Stiavelli[2,3], N. Panagia[3]

Space Telescope Science Institute, 3700 San Martin Drive, Baltimore, MD 21218

C. Marcella Carollo[4]

Department of Physics & Astronomy, The Johns Hopkins University, Baltimore, MD 21218

M. Romaniello[5], I. Heyer and S. Gonzaga

Space Telescope Science Institute, 3700 San Martin Drive, Baltimore, MD 21218

Received ______________; accepted ______________

---

[1]Based on observations with the NASA/ESA Hubble Space Telescope, obtained at the Space Telescope Science Institute, which is operated by Association of Universities for Research in Astronomy, Inc. (AURA), under NASA contract NAS5-26555

[2]On leave from the Scuola Normale Superiore, Piazza dei Cavalieri 7, I-56126 Pisa, Italy

[3]On assignment from the Space Science Dept. of the European Space Agency

[4]Hubble Fellow

[5]also Scuola Normale Superiore, Pisa

ABSTRACT

We present WFPC2 images in the F450W, F606W and F814W filters of the interacting pair of galaxies NGC 454. Our data indicate that the system is in the early stages of interaction. A population of young star-clusters has formed around the late component, and substantial amounts of gas have sunk into the center of the earlier component, where it has not yet produced significant visible star formation or nuclear activity. We have photometric evidence that the star-clusters have strong line emission, which indicate the presence of a substantial component of hot, massive stars which formed less than 5-10$Myrs$ ago.

subject headings: galaxies: elliptical and lenticular, cD — galaxies: individual (NGC 454) — galaxies: star clusters — galaxies: interactions

1. Introduction

Extensive evidence both from the nearby universe and high redshift studies shows that galaxies interact and that interactions can strongly affect the galactic properties and even alter the morphological type. Numerical multi-component simulations (Barnes and Hernquist 1996) have shown that the interstellar gas rapidly sinks into the cores of the interacting galaxies, where it cools and forms stars. Because of their origin, stars formed in this way are not expected to have an angular momentum vector aligned with the main galactic body. Indeed, a significant fraction of elliptical galaxies possesses kinematically decoupled cores (hereafter KDC). However, systematic observations of KDC galaxies with the Hubble Space Telescope (hereafter HST) have shown only indirect evidence for disks and little evidence for young stellar populations in the nuclear regions (Carollo et al. 1997a,b). In addition, the nuclear properties of KDC galaxies are essentially indistinguishable from those of galaxies without (known) KDC nuclei. One possibility is that the phenomena which lead to a KDC actually occur in all galaxies and that they shape their nuclear properties (Carollo et al. 1997b).

To investigate these issues we have studied the interacting system NGC 454 (Arp and Madore 1987). Johansson (1988) describes NGC 454 as a pair consisting of a red elliptical galaxy (Eastern component, E) and a blue irregular or possibly a disk galaxy (Western component, W). To the south of W there are three very blue knots (SW, SE, and S) that were identified by Johansson (1988) as possible young globular clusters. The evidence for the interacting nature of NGC 454 comes from the distorted morphology of both the E and W components, from the fact that both objects are embedded in a common, low surface brightness halo, and from spectroscopic and photometric evidence for a young stellar population in the system.

We observed NGC 454 with the Wide Field and Planetary Camera 2 (hereafter

WFPC2) aboard HST. The observations are described in Section 2. Section 3 is devoted to a description of our data analysis techniques, while our results are discussed in Section 4.

2. Observations

NGC 454 was observed in fine lock during a single orbit on March 6th, 1997. Together with 8 narrow band images of the planetary nebula NGC 2346, these were the first science exposures obtained with WFPC2 after Servicing Mission 2 (hereafter SM2). We obtained, at gain 7, 2$\times$ 500 seconds F450W exposures, 2 $\times$ 140 seconds F606W exposures, and a 200 plus a 400 seconds F814W exposures. Each image was processed with the standard HST WFPC2 pipeline for bias and dark current subtraction, and flat fielding. The flat fields used were those obtained before SM2. We verified that no change could be seen in internal flat fields taken before and after SM2 and that no trend was visible in the sky far from the targets. The two frames available in each filter were combined using the STSDAS IRAF task CRREJ. The central pixel in the elliptical galaxy in the F606W filter, and the innermost 3 and 5 pixels, respectively, in the 200 and 400 seconds F814W exposures, saturated the A/D conversion.

Photometric calibration was carried out in two different ways. When studying young stellar populations around NGC 454 West or areas potentially affected by strong line emission, we considered directly the HST magnitudes, derived applying Holtzman et al. (1995) zero-points to the instrumental magnitudes, and compared them with model calculations in the same WFPC2 magnitude system (see Section 3.2). Instead, when studying the older population of NGC 454 East we converted the magnitudes from the WFPC2 system into the BVI Johnson-Cousins system according to the Holtzman et al. (1995) synthetic calibration. In fact for young stellar systems, the difference in bandpass between the F450W and the F606W filters and the corresponding Johnson filters, and the

effects of dust and emission lines, can make a conversion from the WFPC2 system to the BVI Johnson-Cousins system very inaccurate. The use of the pre-SM2 zero-points and calibration for our post-SM2 data is justified by the throughput stability demonstrated during WFPC2 SM2 activities.

In Figure 1a (Plate XA) we display a combined F450W+ F606W+ F814W image showing the extended common halo and the distorted morphology of both components. In Figure 1b (Plate XB) we show the F450W-F814W color map. Visible are the knots of star formation on the W component as well as the dust in the nucleus of the E component. There are a few blue pixels in the nucleus of E which could be due to recently formed stars.

3. Data Analysis

In the following we report on: *i)* light and color profiles for E, *ii)* point source photometry for W, and *iii)* pixel-by-pixel color-color diagram analysis for various selected areas (shown in Figure 1).

3.1. Light and Color Profiles

Light and color profiles of the E component were derived by using two independent isophote fitting programs both running within IRAF: GALPHOT (Franx et al. 1989) and ELLIPSE (in STSDAS). Both programs gave essentially the same results. The agreement for the F814W profile is excellent for all radii larger than 0.14 arcsec. Inside this radius the profile was affected by the saturated pixels. For the F450W and F606W profiles there were departures within about 2 pixels of the center. In particular, such disagreement seemed to be more serious for the F606W image. The final profiles were obtained by averaging results from the two codes and are shown in Figure 2, where we plot the individual light profiles

(upper left panel) and the F450W-F606W and the F606W-F814W color profiles (bottom panels). The upper right panel contains a color-color plot (B-V vs V-I); for this latter plot the colors were converted to the Johnson-Cousins system so that we could compare them with the theoretical models by Worthey (1994, shown as solid diamonds connected by a solid line). In the figure we also show the reddening line (dotted) and an arrow indicating the direction of contamination by emission lines (W_{eq}(Hα) = 500Å). The points on the upper left of the theoretical models are not an artifact of the isophotal fits, since they are confirmed by inspection of the pixel values in the nuclear region. They are probably due to contamination by emission lines.

The theoretical models belong to an age-metallicity sequence from Worthey (1994). The population models we have considered are: *i)* a 17 Gyrs, [Fe/H]=0.5 population; *ii)* a 12 Gyrs, [Fe/H]=0.25 population; *iii)* a 8 Gyrs, [Fe/H]=0 model, and *iv)* a 5 Gyrs, [Fe/H]=-0.22 model. Models at either constant age or constant metallicity fail to reproduce the observed points, since they produce too small a variation in $B-V$ for a given change in $V-I$. It is only by making the reddest point both older and more metal rich that we can fit the observations. In any case, the youngest, least metal rich models remain redder than the data (particularly in $B-V$). Johansson (1988), on the basis of the global spectral energy distribution of NGC 454-E, claimed that it contained a small fraction of very young stars. An alternative is that NGC 454-E is actually a lenticular galaxy, as suggested by its global colors and the spectrum published by Johansson (1988).

The light profiles of NGC 454-E are not well fitted by an $R^{1/4}$ law alone, or by an exponential alone. An $R^{1/4}$ law can fit well the outer parts (with $R_e \simeq 17''$) but falls below the data inside $\sim 2.5''$. The profiles can be well fitted by the sum of an $R^{1/4}$ plus an exponential law. Given the colors of the object it is likely that this decomposition reflects the existence of two physically distinct components: an $R^{1/4}$ bulge and an exponential disk.

The resulting parameters for the (least affected by dust absorption) V and I filters are: $r_{eV} = 3.1''$, $V_{F606W,bulge} = 13.3$, $r_{eI} = 2.4''$, $I_{F814W,bulge} = 12.7$. The disk component has an exponential scale of $10 \pm 1''$ similar in the two filters. We have also performed a Nuker's law fit (Lauer et al. 1995) of the innermost parts of the F450W and the F606W profiles (the F814W was excluded because of the saturated pixels). We find that the average inner slope is $\gamma = 0.82 \pm 0.05$ and the average break radius is $r_b = 0.70 \pm 0.02$. At the distance of 56 Mpc ($H_0 = 65$km s^{-1} Mpc^{-1}), the bulge absolute magnitude is $M_V = -20.4$. For such an object a nuclear slope of 0.82 is not unusual (Byun et al. 1995).

3.2. Point Source Photometry

The point sources near the two galaxies were identified on the WF2 and WF3 chips in the F814W image (the deepest one) using the DAOFIND package within IRAF. The search was done with a threshold of 5σ above the local background. Subsequently, we carried out aperture photometry on these sources, retaining in the final list only those with a signal-to-noise ratio of at least 3 in all passbands.

At the distance of NGC 454 the effective resolution in the WF chips, $0''.15$, corresponds to a linear size of 41 pc. Therefore, it is most likely that all point sources in our frames be clusters rather than individual stars. This conclusion is confirmed by their bright magnitudes, i.e. $M_V < -9$.

In order to derive the properties of these objects, we computed the time evolution of a single burst of star formation. For this purpose, we used the FRANEC stellar evolutionary tracks (Brocato & Castellani 1993 and Cassisi, Castellani & Straniero 1994) together with the Kurucz (1993) model atmospheres. The model colors were computed in the WFPC2 passbands, using the most up-to-date instrumental response curves available (SYNPHOT

package in STSDAS), thus, enabling us to make a direct comparison between data and theory.

In Figure 3 we plot a color-color diagram for all point sources (a total of 233, of which 56 in the WF2 chip and 177 in the WF3 chip) and compare them to the theoretical evolutionary tracks (heavy solid line, 3 Myrs to 5 Gyrs). We also plot for reference the distribution of colors (i.e. the colors of individual pixels) in galaxies E and W. It is apparent that while E and W essentially lie on the theoretical tracks, all point sources are significantly displaced from them. The effects of reddening and contamination by emission lines were modelled adopting a screen of dust (with the same properties as in the Milky Way) and using Johansson's spectra as templates for emission lines' intensities (Romaniello et al. 1997). The corresponding vectors are indicated with arrows in Figure 3. It is clear that both effects are at work to produce the observed point source displacements. On average, internal reddenings of about $E(B-V) \simeq 0.4$ and Hα equivalent widths in excess of $W_{eq}(H\alpha) \simeq 1000$ Å are required to reproduce the observed colors. The reason why both values are higher than found by Johansson (1988) in his study of the compact objects is that here we resolve the star forming regions much more in detail and, therefore, the contamination of light from older background populations is much less severe. The strong line emission in the spectra of theses clusters imply a very young age for the ionizing stars, namely less than 10 $Myrs$ and, possibly younger than $5 Myrs$. These estimates corresponds to the lifetime of O type stars which are the most important sources of ionizing radiation among young stars (e.g. Panagia 1973) and have lifetimes shorter than 10 $Myrs$ (e.g. Iben 1967).

Even before reddening correction, the F606W magnitudes of these objects are quite bright, ranging from -9.5 up to -14.5 with a median value of -11.3. The luminosity function (see Figure 3) resembles those found for star-clusters in interacting galaxies in more

advanced stages of interaction (Whitmore and Schweizer 1995, Whitmore et al. 1993). The corresponding masses, estimated under the conservative assumption that they consist of young population only, are around 1.8×10^5 $M_\odot$ with a dispersion of a factor of 3 either direction. The total mass in compact clusters turns out to be somewhat higher than 5×10^7 $M_\odot$. This is a little less than 1% of the entire mass of NGC 454 West ($\sim 10^{10}$ $M_\odot$ as estimated from its total visual magnitude, -18.8, and adopting a mass to luminosity ratio of 3). On the other hand, such mass may represent a sizable fraction of the entire gas content of NGC 454 West (say, $M_{gas} \sim 0.1 \times M_{total}$), confirming that star formation induced by galaxy interactions can be very efficient. A detailed discussion of these aspects will be presented in a forthcoming paper (Romaniello et al. 1997).

3.3. Individual Pixel Color Analysis

The properties of the stellar populations in the two galaxies and their uniformity were studied considering the color-color plots of the individual pixels of the two galaxies (see Figure 3). It appears that the stellar populations in the two objects have different properties but are relatively homogeneous within each object. The dispersions of the color distributions for object E are marginally larger than the magnitude error in each pixel. On the other hand, the colors dispersions for object W are about twice as large as the formal error, confirming that object W consists in a complex mixture of stars of different ages, dust, and emission line gas.

In Figure 4 we show a pixel-by-pixel color-magnitude diagram B vs B-I, presented in the form of histogram distributions for six magnitude intervals. The histograms in the three faintest magnitude intervals were computed using frames rebinned in larger pixels (3 by 3 of the original ones) but are still broadened by observational errors (even though only points with a formal error lower than 0.08 magnitudes were considered). The dotted line

represents the color of the sky background. The thin line histograms bluer than the sky refer to NGC 454-W, the thin line histograms redder than the sky represent NGC 454-E. Histograms corresponding to the brighter magnitude intervals are broadened by intrinsic scatter in color. The color of W varies more than that of E, with the brightest pixel being bluer; such trend could be due to either age or reddening effects. The thick line histograms present only in the two fainter intervals correspond to the area belonging to the west tail of E (area T; see Figure 1). Area T has an intermediate color between those of the E and W components, suggesting that it consists in a mixture of stellar populations of both E and W. The color of the tail is very close to the color of the sky, even if the former is much brighter than the latter (the lowest end of the faintest histogram is 0.7 magnitudes brighter than the sky). The close similarity in color suggests that a much more extended and fainter stripped population might occupy vast portions of the image while being very hard to resolve.

4. Discussion and Conclusions

Our observations confirm that the NGC 454 system is in the early stages of an interaction. The star-clusters are very young and contain stars able to provide a very strong UV continuum. It is likely that the most of the emission lines observed by Johansson (1988) in object W are actually produced by the star-clusters. The total mass of the blue, compact clusters is of the order of 10% of the whole interstellar gas of NGC 454-W, indicating a high efficiency of the interaction induced star formation.

Johansson (1988) emission line spectrum of the E component, the blue pixels in the central regions, and the distribution of dust lanes reaching down to the center, provide evidence that gas has sunk into the center of component E. However, our observations do not reveal signs of strong star formation there. Since object E already follows the correlation between nuclear cusp slope and magnitude of the spheroidal component observed for other

elliptical galaxies and bulges (Byun et al. 1996), should the two components merge to form a more massive elliptical galaxy, the cusp slope would have to decrease for the final merger endproduct to continue obeying the correlation. Whether the gas in the core of E will ever go through a star burst phase is hard to predict. Indeed, the emission line spectrum measured by Johansson with its [OIII]λ5007 much stronger than Hβ and its [NII]λ6583 stronger than Hα is more typical of narrow line AGNs than of star forming regions (Veilleux and Osterbrock 1987). Thus, it is possible that we are just witnessing the refueling of a possible AGN engine in the E component.

5. Acknowledgements

We wish to thank Brad Whitmore for a careful reading of the manuscript and the anonymous referee for useful comments. CMC is supported by NASA through the grant HF-1079.01-96a awarded by the Space Telescope Science Institute, which is operated by the Association of Universities for Research in Astronomy, Inc., for NASA under contract NAS 5-26555. This research has made use of the NASA/IPAC Extragalactic Database (NED) which is operated by the Jet Propulsion Laboratory, Caltech, under contract with NASA. MR acknowledges support from DDRF grant 82160.

6. References

Arp H.C., Madore B.F., 1987, "A Catalogue of Southern Peculiar Galaxies and Associations", Cambridge.

Barnes J.E., Hernquist L., 1996, ApJ, 471, 115.

Brocato E., Castellani V.,1993, ApJ 410, 99.

Byun Y.-I., 1996, AJ, 111, 1889.

Carollo C.M., Franx M., Illingworth G., Forbes D.A., 1997a, ApJ, 481, 710.

Carollo C.M., Danziger I.J., Rich R.M., Chen X., 1997b, ApJ in press.

Cassisi S., Castellani V., Straniero O.,1994, AA, 282, 753.

Franx M., Illingworth G., Heckman T., 1989, AJ, 98, 538.

Holtzman J.A., et al., 1995, PASP, 107, 1065.

Iben, I., Jr., 1967, ARAA, 6, 571.

Johansson, L., 1988, AA, 191, 29.

Kurucz R.L., 1993, ATLAS9 Stellar Atmosphere Programs and 2 $km\ s^{-1}$ grid (Kurucz CD-ROM No. 13)

Lauer T.R., et al., 1995, AJ, 110, 2622.

Panagia, N., 1973, AJ, 78, 929.

Romaniello, M., Panagia, N., Carollo, C. M., Stiavelli, M., 1997, in preparation.

Veilleux S, Osterbrock D.E., 1987, ApJS, 63, 295.

Whitmore B.C., Schweizer F., 1995, AJ, 109, 960.

Whitmore B.C., Schweizer F., Leitherer C., Borne K., Robert, C., 1993, AJ, 106, 1354.

Worthey G., 1994, ApJS, 95, 107.

7. Figure Captions

Figure 1: Left Panel: combined F450W+F606W+F814W image of NGC 454. The North is identified by the arrow. The boxes identify the areas discussed in the text. SW, SE, and S are "point" sources discussed by Johansson (1988). We resolve both SW and SE in multiple sources. Right Panel: F450W-F814W color map.

Figure 2: NGC 454 East light profiles and colors. On the upper left panel we show the light profiles in the F450W, F606W, F814W filters. The bottom panels show the F450W-F606W and the F606W-F814W color profiles (left and right respectively). The upper right panel shows a B-V vs V-I plot. The dotted line indicates the effect of reddening while the arrow indicates the effect of line emission in the broad band filters.

Figure 3: The F450W-F606W vs F606W-F814W color-color diagram for the point sources: filled squares, open triangles and crosses denote points with color errors less than 0.12, 0.12-0.20, and 0.20-0.40, respectively (63, 77 and 93 sources, respectively). Theoretical evolutionary tracks (3 Myrs to 5 Gyrs) are displayed as a heavy line. For reference, the colors of individual pixels of components NGC 454-E and NGC 454-W are also plotted. The dashed lines represent the effect of reddening while the dotted line indicates the effect of contamination by emission lines. The scale of such effects is identified by the two arrows. The inset shows the luminosity function in the V_{F606W} magnitude. Histograms have progressively less shading with increasing color uncertainty.

Figure 4: B vs B-I diagram for each pixel in the selected areas of Figure 1, for six intervals one magnitude wide. The dotted line represents the color of the sky. The thin solid line histograms bluer than the sky refer to the object W, the thin solid line histograms redder than the sky represent object E, while the thick solid line histogram, visible only in the two fainter intervals, refers to an area corresponding to the west tail of E and the north of W. The tail of E has a color intermediate between those of E and W.

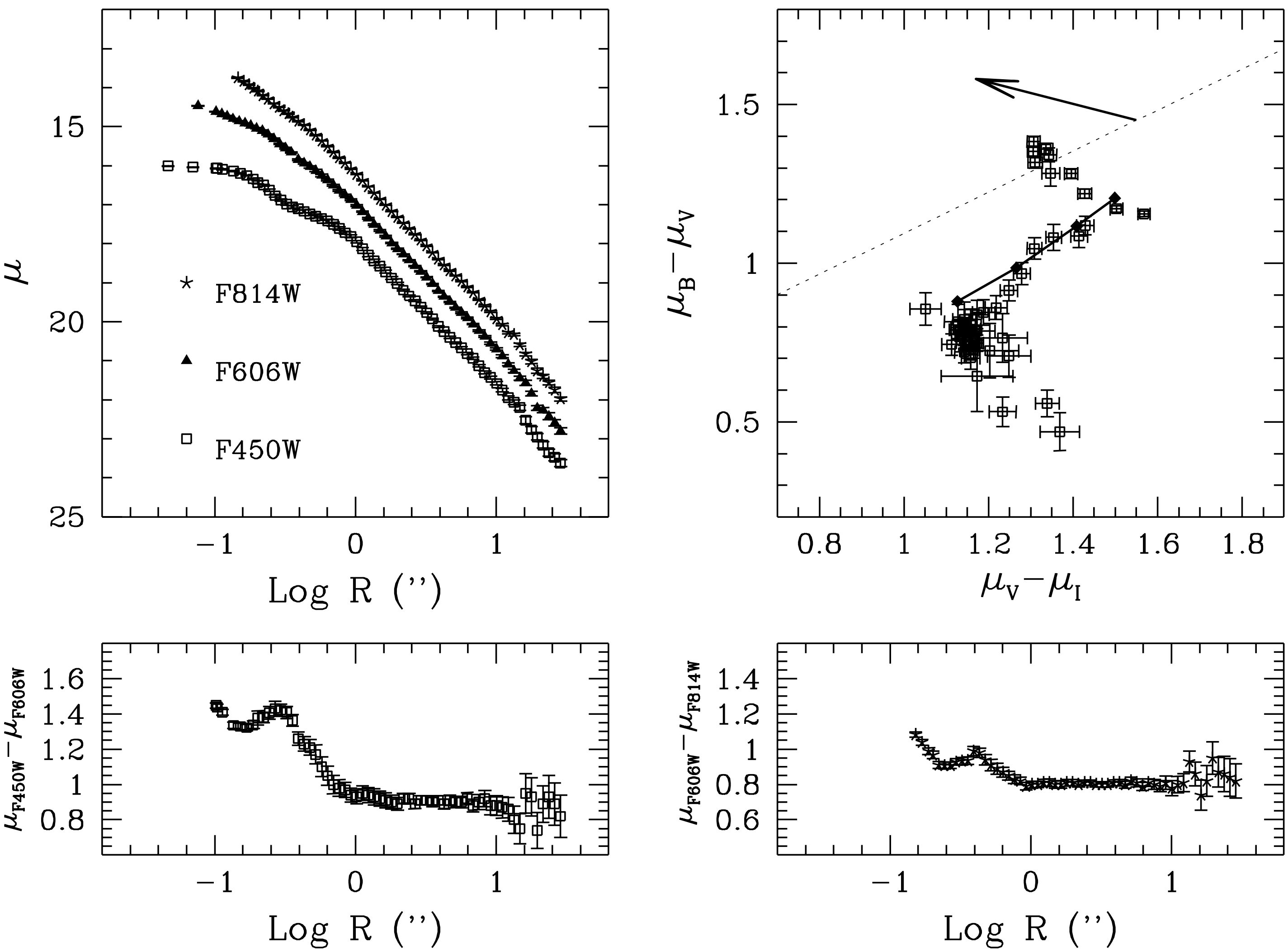

F814W
F606W
F450W
μ
Log R ('')
μB−μV
μV−μI
μF450W−μF606W
μF606W−μF814W

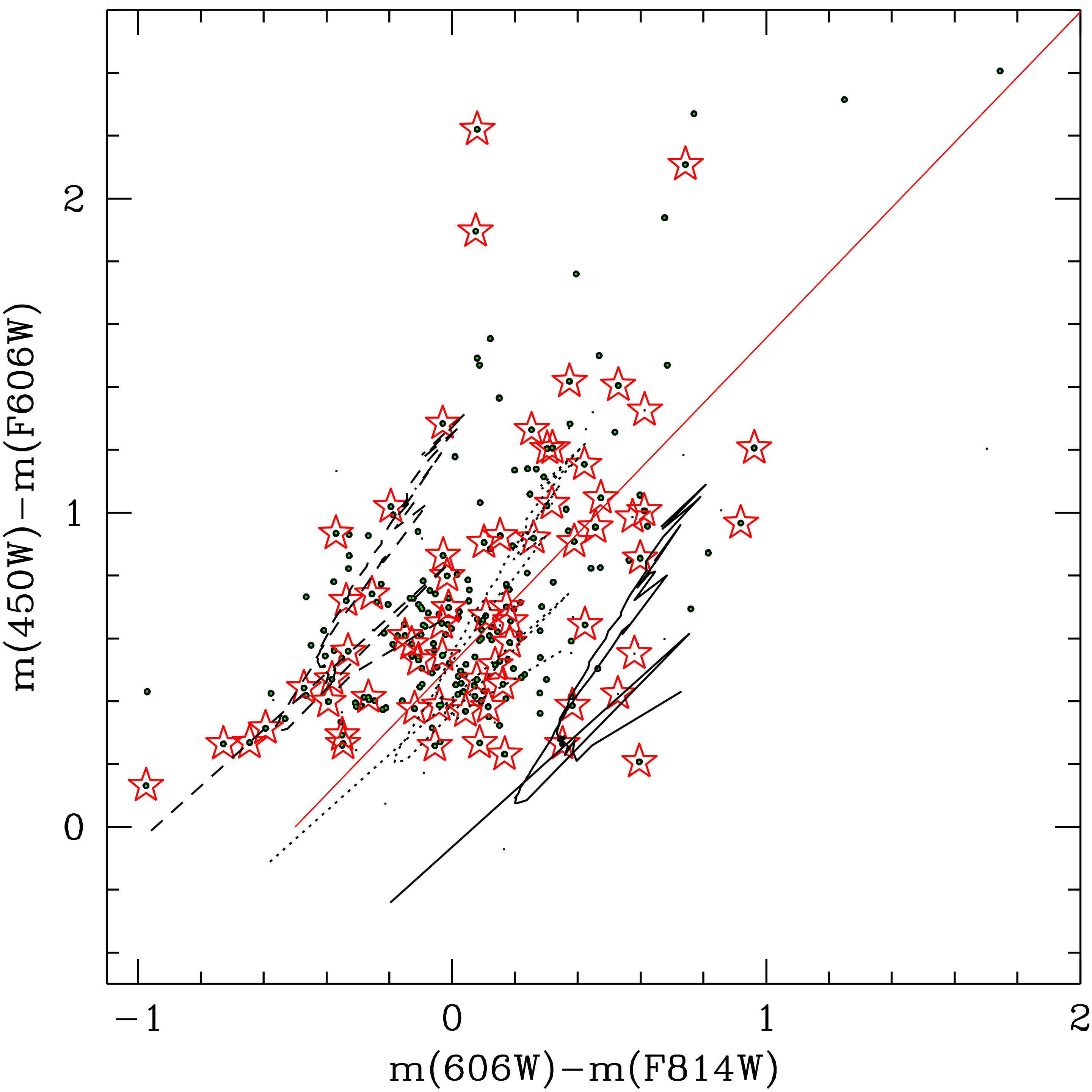

m(450W)−m(F606W)
m(606W)−m(F814W)
−1
0
1
2

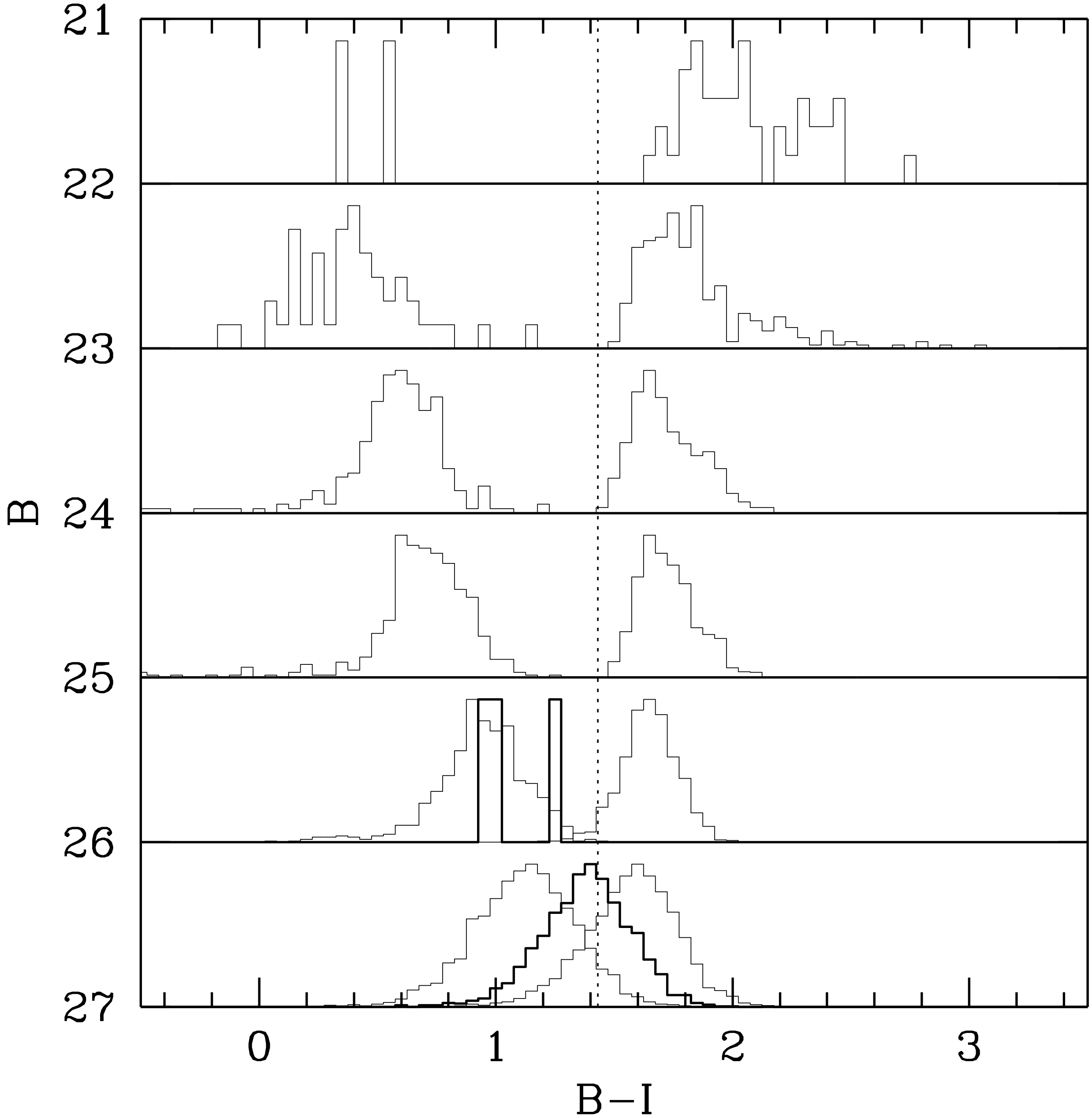

21
22
23
24
25
26
27
B
0
1
2
3
B−I